Proc. of the 9th Intl. Conf. of Asian Society for Precision Engg. and Nanotechnology (ASPEN 2022)
15–18 November 2022, Singapore. Edited by Nai Mui Ling Sharon and A. Senthil Kumar
doi://10.3850/978-981-18-6021-8_OR-06-0086

Towards Effective Powder Reuse in "Large Format Laser Aided Additive Manufacturing" (LAAM)

Clarice Loke[1], Marcin Debowski[1], Sandor Nemeth[1,#], Min Hao Goh[2], Xinying Deng[1], and Shuyun Chng[1]

1 Sustainable & Circular Process Technology (SCPT) Group, Singapore Institute of Manufacturing Technology, 2 Fusionopolis Way, #08-04, Innovis, Singapore 138634
2 Diagnostic and Measurement Unit, Singapore Institute of Manufacturing Technology, 2 Fusionopolis Way, #08-04, Innovis, Singapore 138634
Corresponding Author / Email: sandorn@simtech.a-star.edu.sg, TEL: +65 6419 7422

KEYWORDS: Additive manufacturing, Powder reuse, Powder recycling, 316L stainless steel

With the extensive implementation of additive manufacturing in industry, it becomes imperative to consider the circularity of metal powder for sustainability; keeping the material in circulation through processes such as reuse and recycling. This is especially so in the LAAM process or other large scale production that requires great quantities of material. Improvement in sustainability is ideally achieved by reusing powders directly in LAAM, but potentially hampered by changes in the powder quality due to the preceding build step. A key factor in powder quality deterioration is thermally driven chemical change that is exacerbated by atmospheric exposure in LAAM due to the necessary use of a fairly open system. Understanding the susceptibility of the material to oxidation under varied thermal histories can help to better assess the powder quality for a given additive manufacturing process and the viability of powder reuse. Thus, in this work, we compared the surface properties of 316L stainless steel powders recovered after the LAAM process to samples exposed to varied artificial thermal ageing conditions to correlate thermal history, oxidation level, and powder condition before potential reuse. The chemical changes were induced by high temperature treatment of the powders in air atmosphere and the resulting surface transformation was quantified by elemental analysis using energy dispersive X-ray spectroscopy. The obtained data were used to create a time-temperature-oxidation level map for the stainless steel powder. Separately, the powder recovered from LAAM was evaluated for changes in particle size, surface oxidation level, and the heterogeneity in the particle surface condition. Finally, the virgin powder was characterised to serve as a baseline. It was observed that significant heterogeneity developed in the LAAM process for the collected powder primarily affecting the apparent presence of contaminants, and particle surface oxidation that varied in a broad range due to variation of thermal history among the particles. In contrast, the artificially aged samples were much more homogenous, as expected, and provided a calibration scale to correlate the oxidation level of recovered powder particles with the likely thermal history of the particles. The quantification of the fraction of particles with significant changes in the recovered powder gave a measure of reusability that could be further combined with macroscopic powder properties to support decisions on the reuse conditions of metal powder in the LAAM process.

NOMENCLATURE

LAAM = Large format Laser Aided Additive Manufacturing
3D AM = Three Dimensional Additive Manufacturing

1. Introduction

Additive manufacturing is increasingly being adopted to convert metal powders into high value-added metal parts ("3D printing")[1,2]. Apart from tight process control, the feed powders must be of high purity for successful implementation. This requirement tends to limit the reuse of powders collected after the 3D printing as its changes and impurities, such as oxides, can increase porosity of printed parts and impact the mechanical properties [3-8]. One commonly used approach is to monitor the powder use cycles, optionally combined with mechanical measurements on test parts made from the recycled powders [9,10]. The approach is also frequently combined with blending of virgin and used powders in adequate proportions to achieve a minimum level of mechanical strength [11]. Although these approaches can be used successfully, they add cost to the part fabrication through the making and testing of test specimens, and they do not provide significant insight into the factors that may help with, or prevent successful powder reuse.

Efforts are made to better understand the effects of high temperature exposure during the AM process by evaluating the changes in the metal powder in terms of size distribution as well as surface chemistry [4]. Althoughmuch insight is obtained from these experiments, they usually do not fully account for the heterogeneous nature of the changes in the powder caused by the very steep temperature gradients present during printing.Some particles may be oxidised, while others little changed. The situation is even more

severe in large format laser aided additive manufacturing (LAAM) due to exposure to atmospheric conditions and oxidation since the powder blown using inert gas maybe exposed to some ambient air.

Since the particles of the powder used in LAAM process are not equally affected, the bulk properties of the recovered powder will be an average of the particles where the proper weights in the calculation are expected to be disproportionally large for heat affected and oxidised particles since these would be primarily responsible for defects.

One approach to eliminate the heterogeneity of the powder in the experiments is subjecting the virgin feedstock to a well-defined ageing process, such as thermal treatment, to mimic heating effects during the process [4]. This approach then can provide data to correlate uniform powder properties with printing outcomes as a function of well-defined oxidation level. However, there is still very limited information to link actual recycled powder properties to those well-defined artificially aged samples. Thus, the present work aims to establish a correlation between surface properties of used stainless steel metal powder in the LAAM process,and that changed by artificial ageing by heating the powders under various controlled conditions by focusing on the chemical changes of the surface to aid powder reuse.

2. Materials and Methodology

The powder material was Stainless Steel 316L (AM 316L 20-53, Höganäs)and used for printing in a LAAM process withan in-house developed system. (Ar shielding gas at flow rate of 20•L/min at 2 bar, nominal laser power of 1000 W to 1200W).The portions of the powder that escaped deposition onto the part were recovered for analysis and compared to the virgin powder. Electron micrograph images of these powders are shown in Fig. 1.

Virgin powders were artificially aged in air by placing athin layer sample(<0.5 mm) on a small silicon platform, then lowering it into a preheated furnace (Thermo Scientific™ Lindberg/Blue M™) through its vent hole, for predetermined time periods.

JEOL JSM-IT300 scanning electron microscope (SEM)was used for imaging. It was equipped with energy dispersive X-ray spectroscopy (EDX)detector from Oxford Instruments for elemental analysis. EDX analysis of particles were carried out by limiting the analysis area on the top of the individual particles and avoiding signal collection from the highly sloping sides of the particles.

Selected samples were analysed by X-ray photoelectron spectroscopy (XPS, ESCALab 250Xi, Thermo Scientific, UK) with a 500 µm diameter monochromatic Al K± x-ray (1486.6 eV). Powder was adhered on double-sided carbon tape and loaded into the vacuum chamber for measurement.Elemental depth profiling was performed using 500 eV monoatomic Ar ion sputtering, with 2.5 mm by 2.5 mm sputtering area for 4135 s. Survey spectra were collected between every sputtering cycle to quantify compositional changes. Depth profiling provided average compositions due to the experimental constraints of XPS. Relatively large areas of the sample are scanned, much larger than individual particles, giving an average over the particles.Also, an average over various sputtering depths is obtained as contributions will be included from the top of the particles where the oxide layer may be sputtered fully as well as from the sloping sides of the particles where the cross-section of the oxide layer may be exposed and would persist throughout the sputtering. The sputtering depth was estimated based on reference to Ta_2O_5 sputtering rate at 0.052 nm/s.Data was analysed using Avantage software by Thermo Scientific. Carbon was excluded from the analysis due to use of carbon tape.

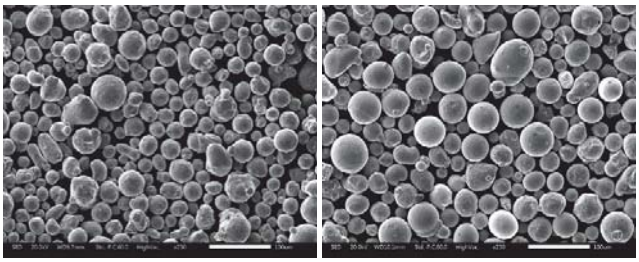

Fig. 1.SEM of virgin powder (left) and recovered powder (right).

3. Results and Discussion

3.1 Analysis of Virgin and Recovered Powder from AM Process

The powders were evaluated by SEM imaging, EDX analysis and XPS analysis. Based on SEM image analysis, the recovered powder had similarnumber average diameter (31.6± 11.6 µm, n=343) to that of the virgin powder (31.5 ±11.7 µm, n=333).

XPS analysis indicated a fully oxidised surface within the analysis depth (~10 nm) consisting of metal oxide and hydroxide species for both virgin and recovered powders. Depth profiling indicated mostly similar behaviour for the virgin and recovered powders with some crucial differences as seen in Fig. 2. The most striking findingis the presence of silicon on the surfaces that rapidly diminishes with depth. Its concentration drops from 9.5 atom percent (at%) to zero within 37 nm sputtering depth for the virgin powder and from 15 at% to nearly zero in 51 nm depth for the recovered powder.The bulk alloy is expected to contain approximately 0.75 weight% (~1.6 at%) silicon.

Mn appears to have nearly constant contribution near 10 at% in the entire depth range tested for both samples. Cr rises from 3 at% to approximately 10 at% at 15 nm depth and remains nearly constant for at least up to 210 nm for both samples. Ni concentration changes from zero at the surface to approximately 9 at% at 40 nm depth then remains essentially constant for up to at least 210 nm depth in the case of the virgin sample while in the recovered sample the Ni content develops in a similar manner but reaches only 7 to 8 at%.

Significant difference is seen in the oxygen and iron concentrations which are essentially mirror images suggesting that the oxygen is primarily associated with iron in the form of Fe_2O_3 (60 at% O in the oxide) and/or FeO (50 at% O in the compound). In the case of the virgin powder, oxygen content drops from 61 at% to 10 at% at 200 nm depth, while the recovered powder changes from 62 at% to 15 at% at 200 nm depth. Comparing the half maximum of oxide

concentration indicates 34 nm for the virgin powder and 43 nm for the recovered powder. The higher oxygen concentration in the recovered powder at 200 nm sputtering depth is likely due to the thicker oxide layer that is exposed as cross-section after the oxide from the top of the particles is sputtered.

Finally, EDX analysis was carried out on individual particles for the virgin and recovered powders. A minimum of 41 particles were checked in most samples of low heterogeneity, and up to 113 spectra were taken in highly heterogeneous samples. EDX indicated an increase of oxygen content, and revealed a heterogenous population in the recovered powder (given in weight percent, wt%). The surface oxygen content was comparable to that of the virgin powder for a significant portion of the particles (40 to 50%) while the rest of the particles displayed a higher level of oxidation (Fig. 3). The averages from the analysis are shown in Table 1. The results revealed that the recovered particles have up to 2.6 times higher average oxygen content in their surface layer compared to the virgin powders. The distribution of other elements in the surface were not substantially different in the two samples.

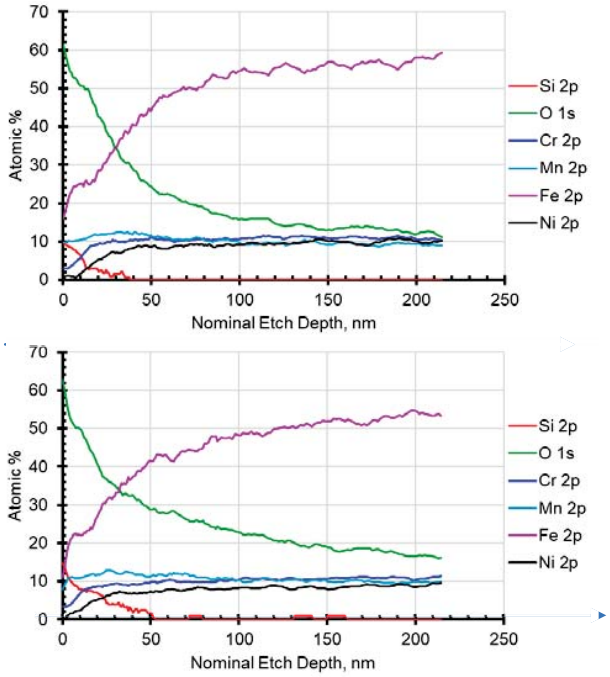

Fig. 2.XPS depth profiling of virgin powder (top) and recovered powder (bottom). The etch depth is nominal, referenced to Ta_2O_5.

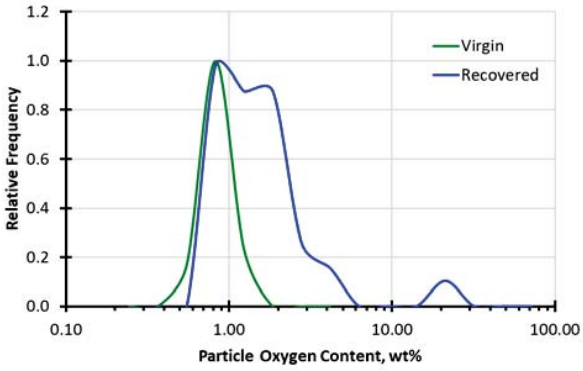

Fig. 3.Oxygen content distribution among particles of virgin and recovered powders.Multimodal distribution is seen in the recovered powder. The highly oxidized peak of recovered powder corresponds to a fully oxidized surface in the entire EDX analysis depth.

Table 1. Comparison of average particlesurface compositions and standard deviations from EDX on a large number of particles.

Element	VirginPowder, wt%	RecoveredPowder*, wt%	RecoveredPowder**, wt%
O	0.86 ± 0.16	1.53 ± 0.81	2.20 ± 3.82
Si	0.77 ± 0.12	0.89 ± 0.17	0.88 ± 0.19
Cr	18.00 ± 0.26	18.09 ± 0.54	18.04 ± 0.61
Mn	1.87 ± 0.22	2.02 ± 0.31	2.04 ± 0.49
Fe	64.44 ± 0.81	63.41 ± 0.97	62.95 ± 2.71
Ni	11.68 ± 0.65	11.67 ± 0.52	11.54 ± 0.95
Mo	2.38 ± 0.22	2.40 ± 0.26	2.34 ± 0.39

* Particles that are measured as fully oxidised in the analysis depth by EDX are excluded from the average

**All analysed particles are included in the average

3.2 Analysis of ArtificiallyAged Powders

Virgin powder samples were lowered in air into a furnace pre-heated to the intended test temperatures (700°C, 900°C, and 1100°C)for set periods(2, 3, 5, and 9 minutes) to promote oxidation. The resulting samples were then tested for surface composition by EDX.

As expected, the oxygen content of the samples increased with temperature in a nearly exponential fashion while the exposure time also influenced the oxidation level, albeit to a lesser extent (Fig. 4, 5).

The surface oxygen concentration was correlated with the heating time at a given temperature by a power curve of the form:

$$C(O, wt\% \text{ at } t) = C(O, wt\% \text{ at } t=0) + a \times t^b$$

where C is the surface concentration of oxygen, C(O, wt% at t=0) =0.85833 (virgin powder, Table 1), t is time in minutes, a and b are fitting parameters.

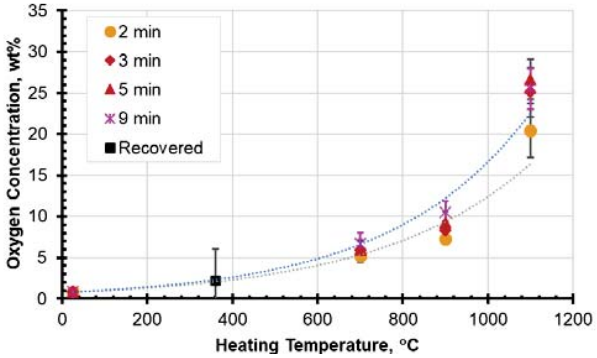

Fig. 4.Surface oxygen content of artificially aged powder samples as a function of exposure temperature and time. The dashed linesare exponential fits for 2 minutes and 9 minutes exposures to highlight the general direction of O concentration changes. The recovered powder was inserted in the plot to coincide with the dotted lines which indicates that the average oxidation level of the recovered powder is comparable to a powder uniformly exposed to approximately 360°C (in air) but the significant error bars also

highlight that the average temperature consists of a wide range of actual ones, room temperature to ~800°C.

The elemental composition of the surface of artificially aged samples were not significantly affected by the thermal treatment (if oxygen was excluded from the calculation) except for samples aged at 1100°C which displayed large variations. The particles in the 1100°C samples additionally developed ridges on the surfaces, suggesting metal oxide crystal formation; and for longer exposure time (>3 minutes) substantial sintering was observed as well. The few very highly oxidised particles in the recovered powder also appeared to have rougher surface than the rest of the particles (Fig. 6).

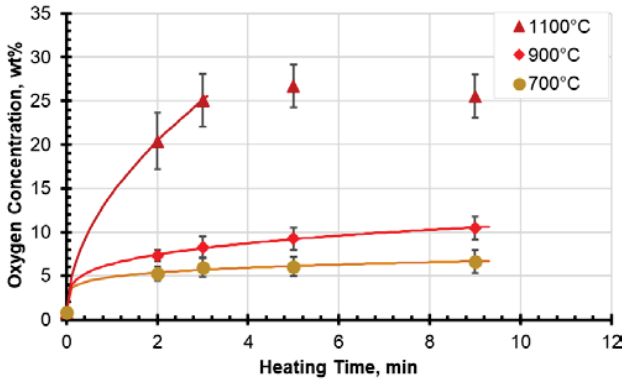

Fig. 5. Evolution of oxygen content in powders exposed to different temperatures at varied durations. The lines are fitted ones as described in the text (at 700°C: a=4.008840, b=0.1689, R^2=0.9992; at 900°C: a=5.509599, b=0.2571, R^2=0.9999; at 1100°C: a=13.53450, b=0.5308, R^2=1.0000). In the case of the data pertaining to 1100°C, full surface oxidation is reached (in the EDX analysis depth) at 5 minutes, thus the fitted line is applied up to 3 minutes only. Comparing the oxygen content of the recovered powder, the plots indicate that the high temperature exposure time is on the order of 1 s or shorter.

Fig 6. Surface roughening of a highly oxidised particles at 1100°C and 2 minutes (left) and roughening of a particle in the recovered powder with 23% surface oxygen content (right, particle highlighted).

4. Conclusions

Surface compositional analysis indicated significant oxidation of recovered LAAM powder. It was also determined that up to half of the powder is not affected while the other half has a wide range of oxidation levels above the desirable range. Comparison to artificially aged samples highlighted that the particles experience modest temperature rise on the average and the rise of the oxygen content is primarily due toa relatively small fraction of highly oxidised particles that experienced high temperature conditions. The findings can be used to develop strategies for the powder recycling such as determining optimum blending ratio with fresh powder based on the distribution of oxidised particles, devising methodologies to separate the high oxygen content particles with the knowledge of the frequency of their occurrence, or reducing the oxidised particle surfaces. Further work is in progress to explore these options.

ACKNOWLEDGEMENT

The authors gratefully acknowledge support from Singapore Institute of Manufacturing Technology (SIMTech) for this work, and contributions with powder samples from colleagues in the Joining and Machining Group of SIMTech.

REFERENCES

1. Pragana, J.P.M., Sampaio, R.F.V., Bragança, I.M.F., Silva, C.M.A., Martins, P.A.F., “Hybrid metal additive manufacturing: A state–of–the-art review”, Adv. Ind. Manuf. Eng., Vol. 2, 100032, 2021.
2. Gisario, A., Kazarian, M., Martina, F., Mehrpouya, M., “Metal additive manufacturing in the commercial aviation industry: A review”, J. Manuf. Syst., Vol. 53, pp. 124-149, 2019.
3. Da Silva, A., et al., “Influence of aluminium powder aging on Directed Energy deposition”, Mater. Des., Vol. 218, 110677, 2022.
4. Saboori, A., et al., “An investigation on the effect of powder recycling on the microstructure and mechanical properties of AISI 316L produced by Directed Energy Deposition”, Mater. Sci. Eng. A ., Vol. 766, 138360, 2019.
5. Heiden, M.J.,Deibler, L.A., Rodelas, J.M., Koepke, J.R., Tung, D. J., Saiz, D.J., Jared, B.H., “Evolution of 316L stainless steel feedstock due to laser powder bed fusion process”, Addit. Manuf., Vol. 25, pp. 84-103, 2019.
6. Yang, X., Gao, F., Tang, F., Hao, X., Li, Z., “Effect of surface oxides on the melting and solidification of 316L stainless steel powder for additive manufacturing,” Metall. Mater. Trans. A, Vol. 52A, pp. 4518-4532, 2021.
7. Santecchia, E., Spigarelli, S., Cabibbo, M. , “Material reuse in laser powder bed fusion: Side effects of laser-metal powder interaction,” Metals, Vol. 10, 341, 2020.
8. He, X., Kong, D., Zhou, Y., Wang, L., Ni, X., Zhang, L., Wu, W., Li, R., Li, X., Dong, C., “Powder recycling effects on porosity development and mechanical properties of Hastelloy X alloy during laser powder bed fusion process,” Addit. Manuf., Vol. 55, 102840, 2022.
9. Hockley, C., Lebed, Y., “Control System and Method for Additive

Manufacturing", European Patent EP3228441A1, 2017.

10. Ambielli, J., "Rapid Synthetic Material Prototyping Process", US Patent Application 2016279878, 2016.
11. Moghimian, P., et al., "Metal powders in additive manufacturing: A review on reusability and recyclability of common titanium, nickel and aluminum alloys", Addit. Manuf., Vol. 43,102017, 2021.